Study of hyperfine-field distributions and the lattice dynamics of $Fe_{50}Ni_{30}Cr_{20}$ alloy by using ^{57}Fe Mössbauer spectroscopy

1999 J. Phys.: Condens. Matter 11 1199

(http://iopscience.iop.org/0953-8984/11/5/008)

J. Phys.: Condens. Matter **11** (1999) 1199–1209. Printed in the UK PII: S0953-8984(99)93825-0

Study of hyperfine-field distributions and the lattice dynamics of $Fe_{50}Ni_{30}Cr_{20}$ alloy by using ^{57}Fe Mössbauer spectroscopy

Debashis Bandyopadhyay

Department of Physics, Indian Institute of Technology, Kanpur-208016, India

Received 1 May 1998, in final form 4 November 1998

Abstract. This paper reports a ^{57}Fe Mössbauer spectroscopic study of a polycrystalline sample of the substitutionally disordered, isostructural (fcc), ternary alloy $Fe_{50}Ni_{30}Cr_{20}$ over the temperature range 10 to 295 K. The data have been analysed in terms of the magnetic phase transitions occurring in the alloy by examining the temperature dependence of the Mössbauer parameters. The Curie temperature has been determined by fitting the average hyperfine-field values obtained at different temperatures. In order to achieve a detailed understanding of the nature of the hyperfine-field distribution corresponding to the Mössbauer spectra of this alloy, the curves representing the probabilities of the hyperfine-field distributions versus the hyperfine field have been refitted by using two independent Gaussians. On the basis of these fits, the local magnetic ordering of this alloy at low temperature has been described. The data on the second-order Doppler shift have been analysed in order to obtain an estimate of the Debye temperature, Θ_D, and a description of the lattice dynamics.

1. Introduction

Studies of magnetic materials exhibiting random mixtures of ferromagnetic and antiferromagnetic interactions have been attracting considerable interest. The iron-rich Fe–Ni binary alloy system represents one such class, and is of paramount importance as far as basic magnetism as well as industrial applications are concerned [1]. Depending upon the relative concentration of Fe and Ni, it shows different magnetic properties. The Fe–Ni alloy having 35 at.% Ni is known as Invar alloy, and that having a Ni concentration of around 75 at.% is known as permalloy. The latter type of alloy is characterized by very high permeability, and is well accepted as being suitable for use in a wide range of industrial applications. The addition of a third alloying element (e.g., Mo, Si, Ge, and Cr) increases the permeability, while cost effectiveness can be achieved by replacing expensive nickel with a cheaper element. In particular, the addition of Cr to Fe–Ni binary alloy can improve the magnetic properties to a great extent [2]. To cite some typical industrial applications, Fe–Ni–Cr alloys are used for manufacturing shield plates of floppy disk drives and video recorders, the iron cores of watches, etc. From the physicist's point of view, the Fe–Ni–Cr ternary alloy system provides several challenging problems. Firstly, no one theory explains the magnetism of 3d-transition-metal alloys. Secondly, the antiferromagnetism of Fe in the fcc γ-phase arises due to negative exchange interaction between the nearest-neighbour (nn) Fe atoms [3]. However, owing to the γ–α phase transformation, it is not possible to study the antiferromagnetic phase of Fe below 1180 K [4]. Addition of Cr or Mn or V stabilizes the γ-phase, and the complete region extending from the antiferromagnetic (Fe-rich) to the ferromagnetic (Ni-rich) form within the

0953-8984/99/051199+11$19.50

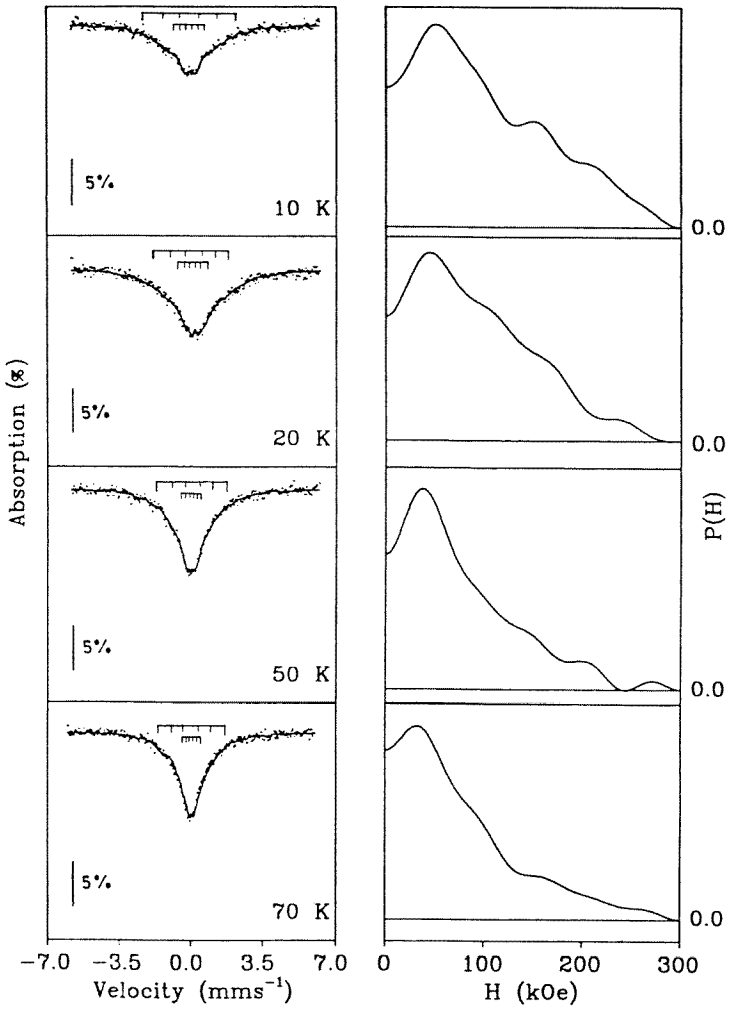

Figure 1. Mössbauer spectra of $Fe_{50}Ni_{30}Cr_{20}$ alloy at different temperatures, and the corresponding hyperfine-field distributions.

same crystallographic fcc phase can be studied [4]. Keeping these aspects in mind, the Fe–Ni–Cr alloys have been studied by different experimental techniques, such as neutron scattering [3–6], magnetic measurements [4, 6], resistivity measurements [7], and magnetoresistance studies [8]. The crystallographic and magnetic phases of this ternary alloy have been described by Majumdar and von Blanckenhagen [4]. Also, the magnetic phase diagram of $Fe_{80-x}Ni_xCr_{20}$ ($10 \leqslant x \leqslant 30$) has been established by Majumdar and von Blanckenhagen [4]. As early as 1963, the hyperfine field in Fe–Ni binary alloy was studied by Johnson *et al* [9], who were followed by other workers using ^{57}Fe Mössbauer spectroscopy in the last three decades [10]. Bendick and Pepperhoff [11] have applied this technique to find the Néel and Curie temperatures of the $Fe_{80-x}Ni_xCr_{20}$ alloys. Other Mössbauer spectroscopic studies of Fe–Ni–Cr alloys have involved the study of the magnetic moments, corrosion protection, and electrochemical processes [12–14]. With this in mind, detailed Mössbauer spectroscopic studies of γ-$Fe_{80-x}Ni_xCr_{20}$ ($x = 30$, 26, 19, and 14) stainless steel alloys over the temperature

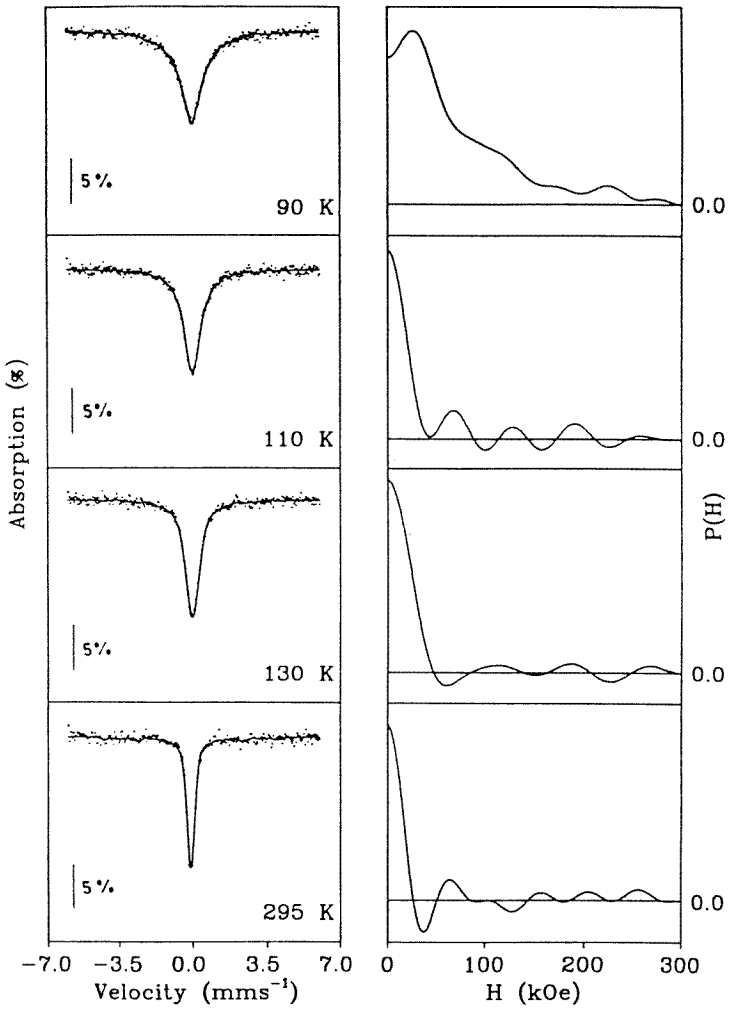

Figure 1. (Continued)

range 10 to 295 K were studied by Bandyopadhyay *et al* [15]. In this paper, a detailed study of the hyperfine-field distributions and lattice dynamics of the above alloy for the composition with $x = 30$ made by using ^{57}Fe Mössbauer spectroscopy has been reported.

2. Experimental procedure

The sample used for the present Mössbauer spectroscopic studies is the same as that used previously in magnetic measurements and neutron scattering experiments [4]. Transmission Mössbauer spectra have been recorded over the temperature range 10 to 295 K. The spectra were obtained using a Mössbauer spectrometer coupled to a multichannel analyser, and operated in constant-acceleration mode. A ^{57}Co source embedded in a rhodium matrix (Amersham International Limited, Amersham, UK) was used. The spectrometer was calibrated using a standard α-Fe foil. The temperature-dependent measurements were made by using an exchange

gas variable-temperature system obtained from JANIS, which is an integral part of a closed-cycle helium cryostat. The analyses of the Mössbauer spectra were carried out with computer programs using two methods. In the first method, a least-squares-fitting computer program employing a Lorentzian shape for the peaks and an iterative procedure was used. In the second method, the procedure of Window [16] was used to obtain the probabilities of the hyperfine-field distributions, $P(H)$, and the average hyperfine field:

$$\langle H\rangle_{\mathrm{W}} = \int H P(H)\,\mathrm{d}H \Big/ \int P(H)\,\mathrm{d}H.$$

3. Results and discussion

In this section, the hyperfine-field distributions of the Mössbauer spectra and the lattice dynamics of the $Fe_{50}Ni_{30}Cr_{20}$ sample will be discussed.

3.1. Study of the hyperfine-field distributions

The magnetic phase diagram [4] indicates that the alloy with $x = 30$ is paramagnetic in the temperature region above 144 K. Mössbauer spectra of this alloy have been measured at 295, 240, 200, 175, 140, 135, 130, 125, 120, 115, 110, 90, 75, 70, 60, 50, 20, and 10 K, and some of them are shown in figure 1 along with their hyperfine-field distributions. For simplicity, all spectra are assumed to be single-component ones, as the experimental accuracy does not warrant more detailed analysis. Each spectrum has been fitted by using the least-squares-fitting method to calculate the overall linewidth of the spectra (Γ_{exp}) and the area under the resonance absorption curve (A) (which has been normalized to the area of the spectra at 10 K and hence has no units). Figures 2(a) and 2(c) show the thermal evolutions of these two parameters. The single average centre shift (δ_{CS}) with respect to the isomer shift of α-Fe has been calculated by using Window's method, and is shown in figure 2(b). Since the spectra cannot be resolved properly even at 10 K, Window's method have been applied to obtain the evolution of the hyperfine-field distributions. Using the results on the hyperfine-field distributions, the average hyperfine field, $\langle H\rangle_{\mathrm{W}}$, has been determined at different temperatures. The variation of $\langle H\rangle_{\mathrm{W}}$ with temperature is shown in figure 2(d). From the curve fit of the temperature dependence of $\langle H\rangle_{\mathrm{W}}$, the value of the paramagnetic–ferromagnetic transition temperature is found to be $T_{\mathrm{C}} = 130 \pm 2$ K. This value is very close to the value of $T_{\mathrm{C}} = 126 \pm 0.2$ K obtained from high-resolution AC susceptibility measurements by Sinha and Majumdar [17]. Both of these values of T_{C} are substantially smaller than that found earlier by Majumdar and von Blanckenhagen [4] from DC magnetization studies. The reason for this is not certain, but it might be due to the different sensitivities of the methods used for determining T_{C} for this intrinsically complex alloy. Each of the above parameters, i.e., Γ_{exp}, A, δ_{CS}, and $\langle H\rangle_{\mathrm{W}}$, obtained from the two different analyses shows a transition zone, where some sudden change of regime occurs. As T decreases, the overall experimental linewidth of the Mössbauer spectra (Γ_{exp}), the normalized area under the resonance curve (A), and the average hyperfine field ($\langle H\rangle_{\mathrm{W}}$) increase sharply, at around 130 ± 2 K, whereas the centre shift starts decreasing. This behaviour can be qualitatively considered as indicative of a magnetic transition, because of the suddenness. It is to be noted that Γ_{exp} increases with the decrease of temperature in the paramagnetic region. This behaviour might be due to relaxation during pre-transitional fluctuations. The method for obtaining the hyperfine-field distributions will now be discussed.

Several methods have been proposed in the literature [16, 18–22] to yield a graph showing the probability of a hyperfine field, $P(H)$, for the measured Mössbauer spectra versus the

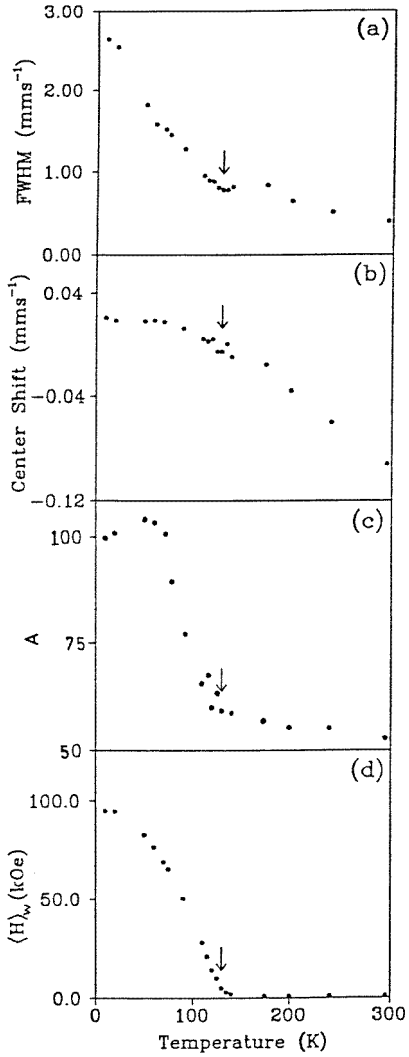

Figure 2. The temperature dependences of (a) the full width at half-maximum, Γ_{exp} (or FWHM), (b) the centre shift (δ_{CS}), (c) the resonance absorption area (normalized) (A), and (d) the average hyperfine field, $\langle H \rangle_W$, of $Fe_{50}Ni_{30}Cr_{20}$ alloy. The vertical arrows show the Curie temperature $T_C = 130$ K as obtained from Mössbauer spectra.

hyperfine field, H. Here, the method developed by Window [16] has been used, by following the procedure suggested by Keller [23]. In this method, $P(H)$ is described in terms of Fourier series. Different parameters have been obtained from the analysis, such as the intensity ratio, b (defined by $I_1{:}I_2{:}I_3 = 3{:}b{:}1$), and the full widths at half-maxima (Γ_W) of the sub-spectra. The isomer shift δ_{IS} and α_{IS} give a direct measure of the correlation between the local isomer shift and the hyperfine field [24]:

$$\delta_{IS}(H) = \delta_{IS}(H_0) - \alpha_{IS}(H - H_0). \tag{1}$$

The parameters are obtained from the best least-squares fit to the measured Mössbauer spectra by solving $N + 1$ simultaneous equations, where N is the number of summation terms in

the Fourier series. The parameters are obtained for the most appropriate value of N, which has been found to be $N = 10$. For $N < 10$, detailed information on the distributions will be lost, whereas $N > 10$ gives rise to unphysical behaviour of $P(H)$. Larger values of the summation terms in the Fourier series tend to fit the statistical fluctuations in the measured spectrum, and hence unavoidable oscillations will occur. The parameters are almost constant for $8 \leqslant N \leqslant 12$. In this region of N, a low-field tail arises which extends up to $H = 0$ for the spectra taken at temperatures less than but close to T_C.

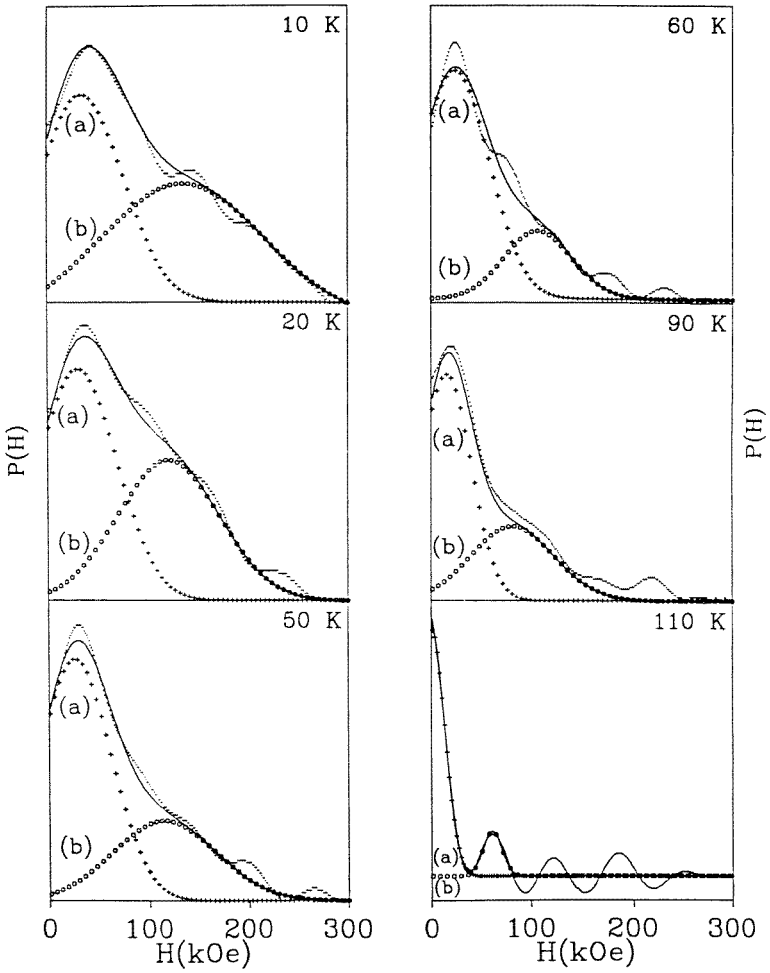

Figure 3. Two-Gaussian fits to the $P(H)$ distribution versus H curves at different temperatures. Curves (a) represent the low-field-side Gaussians (+) and curves (b) the high-field-side Gaussians (○).

Hyperfine-field distributions obtained from Window's method and the corresponding fitted Mössbauer spectra are shown in figure 3. Since low-temperature Mössbauer spectra are broad and are not well resolved, the distributions show a wide spread from 0 to 300 kOe with a non-zero value of $P(H)$ at $H = 0$. To understand the nature of the hyperfine-field distributions in detail, it is necessary to consider the nature of the sample used for the present experimental studies. In the Fe–Ni–Cr system, six different pair interactions are present

[3]. The interaction between Fe and Fe and that between Cr and Cr are antiferromagnetic, whereas there is ferromagnetic interaction between Ni and Ni, between Fe and Ni, between Fe and Cr, and between Ni and Cr. The values of the corresponding exchange integrals have been calculated by Men'shikov *et al* [3]. Magnetic phase diagram investigations [4] and several other experimental studies [4, 17] show a paramagnetic–ferromagnetic phase transition in $Fe_{50}Ni_{30}Cr_{20}$ alloy at low temperature. Therefore, it is logical to consider that below the Curie temperature the bulk shows a ferromagnetic behaviour although the interactions between Fe and Fe and those between Cr and Cr are antiferromagnetic. In other words, ferromagnetic interactions dominate over antiferromagnetic interactions. The ferromagnetic interactions are the consequence of long-range interactions of like spins in a lattice that is identical with the atomic lattice. With decreasing temperature, the intensity of the long-range ferromagnetic interaction and the degree of short-range spin ordering increase. In this system, the Fe, as atoms having an Fe nearest-neighbour environment, interact antiferromagnetically. Therefore the sample looks like antiferromagnetic (AFM) clusters in a ferromagnetic (FM) matrix, where the local environment of the former iron sites is 'Fe rich' and that for the latter sites is 'Fe poor' [25, 26]. Alternately, if the number of such antiferromagnetic (AFM) clusters is negligible, then the sample can be viewed as having two non-equivalent iron sites representing the spin localization in the finite (or short-range) ferromagnetic (FM) spin clusters, and an infinite (or long-range) ferromagnetic matrix. Such magnetically inhomogeneous coexistences are reflected in the wide distributions of the Mössbauer hyperfine fields. The local magnetic moment in FM spin clusters is usually lower than that in the FM matrix, but it is large in a FM matrix [27]. The bimodal nature of the distributions is due to the existence of atoms with low internal fields [28]. Keeping all of these points in mind, the hyperfine-field distributions have been fitted using two independent Gaussians having different positions and widths, following Weiss [29], and the results are shown in figure 3. On the basis of the above discussion, the two Gaussians on the low- and high-field sides of the $P(H)$ distributions have been assigned as the Gaussians originating from the Fe atoms in the 'low-field clusters' and in the 'high-field FM matrix' respectively. It is to be noted that even after decomposing the hyperfine-field distributions into two Gaussians, the value of $P(H)$ at $H = 0$ is still very high. This is due to the fact that the Fe atoms in low-field clusters, which are responsible for the low-field Gaussian, have hyperfine fields which are very small, and hence are not resolved. So they contribute a non-zero value of $P(H)$ at $H = 0$ in the hyperfine-field distributions, as does the presence of a paramagnetic phase. To check the validity of using the two-Gaussian fit to the hyperfine-field distributions to segregate the clusters from the FM matrix, another approach has been followed.

Table 1. Different parameters for the Mössbauer spectra obtained from the two analyses.

T (K)	Γ_W (mm s^{-1})	Γ_{cl} (mm s^{-1})	Γ_{FM} (mm s^{-1})	$\langle H\rangle_W$ (kOe)	$\langle H\rangle_{cl}$ (kOe)	$\langle H\rangle_{FM}$ (kOe)	b_W	b_{cl}	b_{FM}	χ^2_W	χ^2_{Fit}
10	0.34	0.34	0.32	95	41	52	2.0	1.8	2.1	1.8	1.2
20	0.35	0.32	0.30	94	45	48	2.3	1.7	2.2	1.4	1.4
50	0.34	0.30	0.28	84	51	30	2.5	1.8	2.4	1.8	1.9
60	0.35	0.25	0.24	78	53	27	2.5	2.1	2.3	2.0	1.7
90	0.36	0.24	0.23	50	35	14	2.6	2.6	2.5	3.1	2.3
110	0.33	0.26	0.24	28	22	5	2.9	2.9	2.8	3.4	2.6
Errors:	±0.05 (mm s^{-1})	±0.05 (mm s^{-1})	±0.01 (mm s^{-1})	±3 (kOe)	±3 (kOe)	±3 (kOe)	±0.01	±0.01	±0.01		

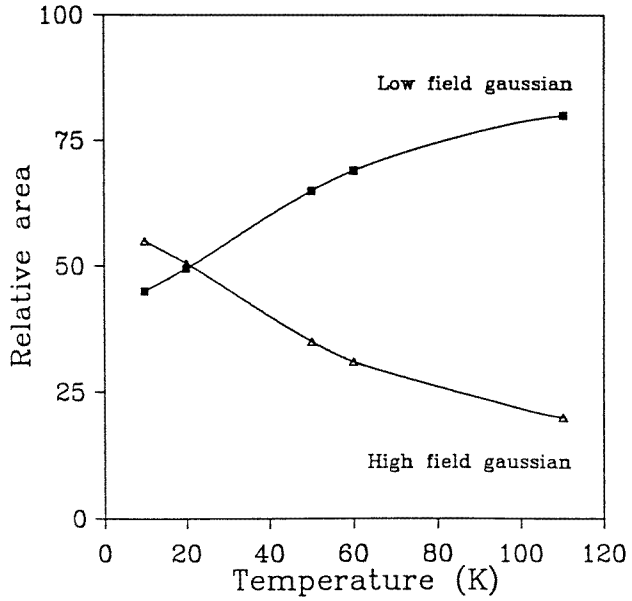

Figure 4. The percentage variation of the normalized area for two Gaussians at different temperatures.

In the second approach, the Mössbauer spectra below the Curie temperature have been refitted with two Lorentzians corresponding to (i) the clusters (a narrow Lorentzian) and (ii) the FM matrix (a wide Lorentzian). The line positions of the two Lorentzians are shown above the fitted experimental spectra in figure 3. The upper lines correspond to the Lorentzian representing the FM matrix and the lower ones are due to clusters. Different parameters of these two sub-spectra are then compared to those obtained from the analysis made by Window's method, and these are shown in table 1. The linewidth obtained from Window's method (Γ_W) is almost always constant and equal to 0.34 mm s^{-1}. The linewidth corresponding to the clusters (Γ_{cl}) and the FM matrix (Γ_{FM}) decreases continuously from T_C. The nature of the variation of the average hyperfine fields corresponding to the clusters and the FM matrix, i.e. $\langle H\rangle_{cl}$ and $\langle H\rangle_{FM}$, is the same as that of $\langle H\rangle_W$ obtained from Window's method. The variation of b is nearly the same as that of b_{FM}, whereas b_{cl} decreases below b_W and b_{FM}. The χ^2-values are also almost the same below the Curie temperature T_C. From the variation of the above parameters, it is clear that the two-Gaussian fits to the hyperfine-field distributions are well supported by the spectral fit made by using two Lorentzians, corresponding to low-field clusters and the high-field FM matrix. The variations of $\langle H\rangle_W$, $\langle H\rangle_{cl}$, and $\langle H\rangle_{FM}$ with temperature can be understood on the basis of the data given in table 1. The sum of $\langle H\rangle_{cl}$ and $\langle H\rangle_{FM}$ is approximately equal to $\langle H\rangle_W$. The natures of the variations of $\langle H\rangle_W$ and $\langle H\rangle_{FM}$ are same, whereas $\langle H\rangle_{cl}$ decreases with decrease in temperature. The variation of the normalized areas of the two sub-Gaussians along with the variations of their peak positions are shown in figure 4 and figure 5 respectively. At a temperature of 10 K, the area of the low-field Gaussian is 45%, whereas at the temperature of 110 K it is 80%. It is clear from figure 4 that as temperature increases, the low-field clusters increase in number at the cost of loss of the high-field FM matrix. The hyperfine fields corresponding to both peaks increase with decreasing temperature, as shown in figure 5. This is probably due to the freezing of the transverse components of the spins in both the clusters and the FM matrix. The same phenomena have been found by

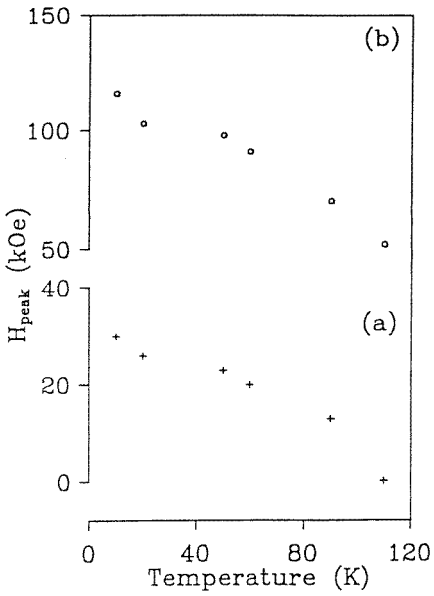

Figure 5. The variation of H_{peak} for the two Gaussians with temperature. (a) The crosses represent the low-field-side Gaussian. (b) The circles represent the high-field-side Gaussian.

Kunitomi *et al* [30] for Cr–Fe alloy. It is well known that Mössbauer spectroscopy can 'sense' a spin-glass transition well above the actual spin-glass transition [31]. Therefore the nature of figure 5 might be due to the trace of a spin-glass transition somewhere at low temperature in this alloy.

3.2. Study of the lattice dynamics

To study the lattice dynamics of the $Fe_{50}Ni_{30}Cr_{20}$ sample, the values of the centre shift (δ_{CS}) of the Mössbauer spectra taken at different temperatures have been measured. The variation of the centre shift (δ_{CS}) with temperature is shown in figure 2(b). It is well known that the centre shift is the sum of the chemical isomer shift (δ_{IS}) and the contribution from the second-order Doppler shift (δ_{SOD}). The centre shift, δ_{CS}, can be expressed as

$$\delta_{CS} = \delta_{IS} + \delta_{SOD}. \tag{2}$$

A non-zero contribution from the second term of the above expression arises due to the relativistic effect whenever the source and absorber are at different temperatures, and is also known as the thermal shift. This temperature-dependent part of the centre shift is caused by the time dilation resulting from the thermal motion of the γ-ray emitting and absorbing nuclei. If $\langle v^2 \rangle$ is the mean square velocity of the Mössbauer atom in the lattice, then δ_{SOD} can be expressed as

$$\delta_{SOD} = -\langle v^2 \rangle / 2c. \tag{3}$$

In this way the Doppler shift is related to the lattice dynamics of Debye solids. The temperature dependence of the centre shift gives information about the vibrational states of Debye solids. To calculate the Debye temperature, Θ_D, the experimental data relating to the values of the

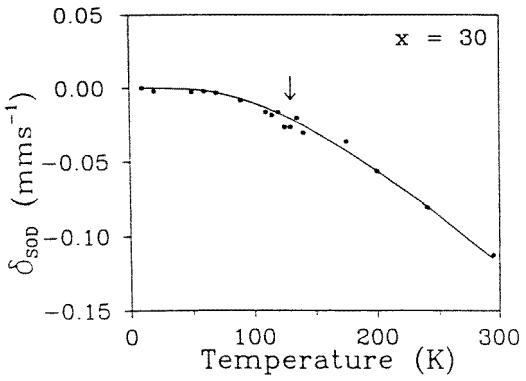

Figure 6. A curve fitted (continuous curve) to the second-order Doppler shift values (δ_{SOD}) for determining the Debye temperature (Θ_D) of $Fe_{50}Ni_{30}Cr_{20}$ alloy. The vertical arrow represents the Curie temperature (T_C).

centre shift have been fitted by using the following equation:

$$\delta_{CS}(T_1) - \delta_{CS}(T_2) = \frac{9k}{2Mc}\left[T_2\left(\frac{T_2}{\Theta_D}\right)^3 \int_0^{\Theta_D/T_2} \frac{x^3}{x^3-1}\,dx - T_1\left(\frac{T_1}{\Theta_D}\right)^3 \int_0^{\Theta_D/T_1} \frac{x^3}{x^3-1}\,dx\right] \tag{4}$$

where it has been assumed that the isomer shift (δ_{IS}) is independent of the temperature and T_2 is the lowest temperature. By using the minimum-standard-deviation method, the experimental data relating to the values of the centre shift, δ_{CS}, have been fitted as shown in figure 6, which gives the value of Θ_D as 461 K. It is clear from figure 6 that there is hardly any change in δ_{SOD} below T_C. This indicates that below T_C there is no effect from the electronic structural anomaly or phonon softening of the $Fe_{50}Ni_{30}Cr_{20}$ alloy. The softening corresponds to the case of lattice vibration when the average velocity decreases. Again, the expression for $\langle v^2 \rangle$ which has been used for fitting the experimental data holds for a harmonic crystal. So, one could conclude that below T_C the vibrational motion of Fe atoms remains harmonic. The average velocity decreases below T_C, as discussed earlier. The decrease of $\langle v^2 \rangle$ reflects the absence of vibrational instabilities in the lattice below T_C.

4. Conclusions

The results obtained from the study of hyperfine-field distributions and the lattice dynamics of $Fe_{50}Ni_{30}Cr_{20}$ alloy made by using the ^{57}Fe Mössbauer spectroscopic technique can be summarized as follows:

(a) The magnetic hyperfine-field distribution is bimodal in the sense that the low-field component appears as a shoulder on the low-field side along with the main hyperfine field.

(b) The total hyperfine field is due to the contribution of low-field spin clusters and the high-field FM matrix. As the temperature decreases the low-field spin fraction decreases, whereas the high-field spin fraction increases at the cost of loss of some of the low-spin fraction. The nature of the variations of the peak positions of the two Gaussians indicates probable freezing of the transverse components of the spins in clusters and the FM matrix.

(c) The Debye temperature calculated from the values of the centre shift at different temperatures has a value of 461 K. From the nature of the fitted curve, one can conclude that Fe atoms remain harmonic, and no phonon softening is observed below the Curie temperature. This behaviour could be due to a phase transition from a paramagnetic to a ferromagnetic state.

Acknowledgments

The author wishes to thank Professor A K Majumdar and Dr Sandeep Singh for valuable discussions. He also would like to thank Miss Antara Samanta for her help in this work.

References

[1] Ishikawa Y and Miura N (ed) 1991 *Physics and Engineering Applications of Magnetism* (Berlin: Springer)
[2] Nakamura Y 1994 *Hyperfine Interact.* **83** 55
[3] Men'shikov A Z, Sidorov S K and Teplykh A Ye 1979 *Fiz. Met. Metalloved.* **45** 42
[4] Majumdar A K and von Blanckenhagen P 1984 *Phys. Rev.* B **29** 4079
Majumdar A K and von Blanckenhagen P 1983 *J. Magn. Magn. Mater.* **40** 227
[5] Men'shikov A Z and Teplykh A Ye 1979 *Fiz. Met. Metalloved.* **44** 78
[6] Nathans R and Pickart S J 1964 *J. Phys. Chem. Solids* **25** 183
[7] Banerjee S and Raychaudhuri A K 1992 *Solid State Commun.* **83** 1047
Nath T K and Majumdar A K 1996 *Phys. Rev.* B **53** 12 148
[8] Banerjee S and Raychaudhuri A K 1993 *J. Phys.: Condens. Matter* **5** L295
[9] Johnson C J, Ridout M S and Cranshaw T E 1963 *Proc. Phys. Soc.* **81** 1069
[10] Hesse J 1989 *Hyperfine Interact.* **47** 357 and references therein
See also:
Freeman A J and Shimizu M 1979 *J. Magn. Magn. Mater.* **10** 109
[11] Bendick W and Pepperhoff W 1981 *J. Phys. F: Met. Phys.* **11** 57
[12] Ghafari M, Okiyama T, Takemato T, Kawai Y and Nakamura Y 1993 *Nucl. Instrum. Methods* B **76** 37
[13] Vertes A 1989 *Hyperfine Interact.* **45** 113
[14] Kuzmann E, Czako-Nagy I, Vertes A, Chisholm C U, Watson A, El-Sharif M K, Kerti J and Konczos G 1989 *Hyperfine Interact.* **45** 397
[15] Bandyopadhyay D 1996 *PhD Thesis* Indian Institute of Technology, Kanpur
Bandyopadhyay D, Singru R M and Majumdar A K 1999 *Hyperfine Interact.* at press
[16] Window B 1971 *J. Phys. E: Sci. Instrum.* **4** 401
[17] Sinha G and Majumdar A K 1998 *J. Magn. Magn. Mater.* **185** 18
[18] Saron T E and Tsuei C C 1971 *Solid State Commun.* **9** 1923
[19] Saron T E and Tsuei C C 1972 *Phys. Rev.* B **5** 1047
[20] Logan L and Sun E 1976 *J. Non-Cryst. Solids* **20** 285
[21] Hesse J and Rübartsch R 1974 *J. Phys. E: Sci. Instrum.* **7** 526
[22] Vincze I 1978 *Solid State Commun.* **25** 689
[23] Keller H 1981 *J. Appl. Phys.* **52** 5268
[24] Chien C L and Chen H S 1979 *J. Appl. Phys.* C **2** 118
[25] Saito N, Hiroyoshi H, Fukamichi K and Nakagawa Y 1986 *J. Phys. F: Met. Phys.* **16** 911
[26] Read D A, Hallam G C and Chirwa M 1989 *J. Magn. Magn. Mater.* **82** 83
[27] Read D A, Moyo T, Suad J, Dunlop R A and Hallam G C 1989 *J. Magn. Magn. Mater.* **82** 87
[28] Mossish A H, Pollard R J, Wronski Z S and Calka A 1985 *Phys. Rev.* B **32** 7528
[29] Weiss R J 1963 *Proc. Phys. Soc.* **82** 291
[30] Kanitomi N, Nakai Y, Tsuge S, Yamamoto N and Fujita K 1986 *Hyperfine Interact.* **28** 515
[31] Meyer C, Hartmann-Boutron F, Gros Y and Campbell I A 1985 *J. Magn. Magn. Mater.* **46** 254